



# Ultrasonic-Enhanced Laser Cladding: Improving Microstructure and Performance Through Synergistic Processing Techniques



Xinsheng Wang<sup>1</sup> , Yang Zheng<sup>1</sup> , Zhihai Cai<sup>2</sup> , Xian Du<sup>2\*</sup> , Jian Liu<sup>2</sup>, Haidou Wang<sup>2</sup>

<sup>1</sup> Hennan Key Laboratory of Intelligent Manufacturing of Mechanical Equipment, Zhengzhou University of Light Industry, 430002 Zhengzhou, China

<sup>2</sup> National Engineering Research Center for Remanufacturing Academy of Armored Forces Engineering, 100072 Beijing, China

\* Correspondence: Xian Du (30245052@qq.com)

Received: 07-20-2024

Revised: 09-09-2024

Accepted: 09-17-2024

**Citation:** X. S. Wang, Y. Zheng, Z. H. Cai, X. Du, J. Liu, and H. D. Wang, "Ultrasonic-enhanced laser cladding: Improving microstructure and performance through synergistic processing techniques," *Precis. Mech. Digit. Fabr.*, vol. 1, no. 3, pp. 111–130, 2024. <https://doi.org/10.56578/pmdf010301>.



© 2024 by the author(s). Published by Acadlore Publishing Services Limited, Hong Kong. This article is available for free download and can be reused and cited, provided that the original published version is credited, under the CC BY 4.0 license.

**Abstract:** Laser additive manufacturing, a pivotal technology in advanced manufacturing, is extensively applied in the restoration industry. However, its development has been hindered by challenges such as residual stress and excessive grain size during the manufacturing process. The integration of ultrasonic enhancement technology with laser cladding has emerged as a prominent research direction, offering significant improvements in the quality and performance of the cladding layer. This review focuses on two primary approaches: ultrasonic-enhanced synchronous laser cladding and ultrasonic strengthening as a post-processing method. The ultrasonic processes discussed include ultrasonic vibration, ultrasonic rolling, ultrasonic impact, and their composite variants. Each method is evaluated for its ability to modify the microstructure, alleviate defects, and enhance the mechanical properties of the cladding layer. While ultrasonic enhancement during synchronous laser cladding primarily facilitates greater molten pool agitation, post-processing techniques induce severe plastic deformation on the surface of the cladding layer. Both approaches have been shown to reduce residual stress, refine grain structure, and improve surface hardness. The underlying mechanisms governing these improvements, particularly microstructural evolution and grain refinement, are examined in detail. Additionally, the potential advantages and limitations of each ultrasonic introduction method are discussed. Finally, the application prospects and future development trends of ultrasonic-enhanced laser cladding are explored, with particular attention to the role of ultrasonic technology in enhancing the durability, wear resistance, and corrosion resistance of cladding layers. The synergy between ultrasonic techniques and laser cladding promises to expand the potential of additive manufacturing in both industrial and repair applications.

**Keywords:** Laser cladding; Ultrasonic impact treatment; Surface strengthening; Residual stress; Plastic deformation; Grain refinement

## 1 Introduction

In the engineering field, some core components such as turbine blades [1], crankshafts [2, 3], and heavy-duty gears [4] are exposed to harsh conditions such as high temperatures and high-impact loads, making them prone to damage such as wear, corrosion, and fracture [5–7]. Failure to repair them in a timely manner leads to severe economic losses. Compared to other surface treatment technologies (such as cold spraying [8, 9], thermal spraying [10, 11], and chemical vapor deposition [12, 13]), laser cladding technology has recently become the most common surface reinforcement and remanufacturing repair technology in the industrial manufacturing sector [14]. It is widely applied in fields such as mining machinery, automotive manufacturing, and aerospace industries [15, 16]. Laser cladding technology uses high-energy laser beams and alloy powders to reinforce and repair the surface of workpieces, producing a dense, uniform cladding layer with high hardness, wear resistance, and corrosion resistance, thus achieving an overall improvement in material performance. Compared to traditional processing methods, laser cladding technology requires only a small amount of alloy powder to produce high-quality coatings, significantly reducing raw material consumption. Additionally, laser cladding technology is widely applied due to its notable advantages, such as good metallurgical bonding with the substrate, smaller heat-affected zones, low dilution rates, high production efficiency,

and good controllability [17, 18]. However, the unique advantages of laser cladding technology also impose stricter requirements and higher expectations on the performance of the cladding layer. The process parameters during laser cladding have a significant impact on the formation quality of the coating. Improper parameters can lead to defects such as pores and cracks in the coating. For instance, when titanium alloy coatings are prepared on low-carbon steel using laser cladding technology, increased scanning speeds lead to higher amounts of unmelted titanium powder and defects like pores in the coating, whereas decreased scanning speeds result in longer laser spot dwell times, higher line energy density applied to the substrate, and improved wear resistance of the titanium alloy coating due to enhanced diffusion of Fe atoms [19]. Given the brief existence of the melt pool during the laser cladding process and the interrelated effects of multiple parameters, adjustments relying solely on process parameters are challenged and have limited effectiveness, making it difficult to ensure coating quality. Additionally, due to the rapid cooling and heating characteristics of laser cladding, gases within the melt pool cannot escape before solidification, leading to a high number of pores in the coating. During solidification, significant temperature gradients exist, and the difference in thermal expansion coefficients between the substrate and the cladding material creates residual tensile stresses at the surface, causing premature cracking or even delamination of the cladding layer, which reduces the service life of the workpiece. This represents a technological bottleneck that restricts the development of laser cladding.

Several scholars conduct related research, such as Wang et al. [20], who applied 3Cr14Mo powder onto the surface of 9Cr18 stainless steel through laser cladding and find that post-heat treatment (PHT) significantly increases coating hardness, while subsequent low-temperature treatment (CT) can further enhance coating hardness. However, the long heat treatment cycle makes it difficult to implement for large components that are hard to disassemble. Li et al. [21] incorporated Mo elements into the AlCoCrFeNi-TiC coating and find that as the Mo content increases, the coating hardness is elevated from 611.9 HV0.1 to 822.6 HV0.1, but the cost and issues with microcracking limit its further application.

However, these methods do not achieve ideal results. Therefore, exploring an effective reinforcement technology to enhance laser cladding layer performance and address existing issues is of significant practical importance. The combination of ultrasonic reinforcement technology with laser cladding provides new approaches for coating application and performance [22–24]. This combination can address issues such as uneven coating structure, high residual stress, and poor formation quality, thereby meeting the precision and performance requirements for practical applications. This paper is initiated from the perspective of ultrasonic-assisted synchronous laser cladding technology and ultrasonic strengthening as a post-treatment method. The effects of ultrasonic vibration, ultrasonic rolling, and ultrasonic impact, along with their combined processes, on the laser cladding layer are mainly introduced, and the future development trends of ultrasonic strengthening processes are discussed.

## 2 Ultrasonic Enhanced Synchronous Laser Cladding Technology

### 2.1 Ultrasonic Vibration Assisted Laser Cladding

To improve the quality of the cladding layer, externally assisted laser cladding technology is being established as a new direction of research in this field [25]. Ultrasonic vibration, as an auxiliary field, is applied during the solidification process of molten metal. The ultrasonic vibration system primarily consists of an ultrasonic generator, ultrasonic transducer, sonotrode, and vibrating head. Figure 1 shows both contact ultrasonic vibration and non-contact ultrasonic vibration. In the contact ultrasonic system, the vibrating head is in direct contact with the substrate, allowing ultrasonic waves to be transmitted from the substrate to the molten pool during the cladding process, while in the non-contact ultrasonic system, the vibrating head acts on the molten pool through air transmission. Ultrasonic vibration not only alters the flow direction and temperature field distribution within the melt pool but also regulates the growth of the microstructure and the distribution of elements during the solidification of the melt pool [26–29]. The nucleation and growth conditions of grains determine the microstructure, and the synergistic effects of ultrasonic cavitation and acoustic streaming influence the growth of the microstructure in the melt pool, thereby disrupting the growth of coarse columnar dendrites and refining the microstructure [30]. The mechanical effects, cavitation effects, and acoustic streaming effects induced by ultrasonic vibration collectively alter the undercooling and nucleation rate during solidification, thereby affecting the crystallization of the molten metal. Zhuang et al. [31] prepared 316L stainless steel coatings using ultrasonic-assisted laser cladding technology, and it is found that ultrasonic vibration improves the macro morphology and mechanical properties of the coatings. As shown in Figure 2, ultrasonic vibration energy is converted into internal energy, resulting in the presence of significant high-strain regions within the coating. This promotes an increase and rearrangement of dislocations within the original grains, leading to the formation of numerous low-angle grain boundaries inside the grains. As dislocation slip occurs, dislocations entangle to form dislocation walls and overlap to create low-angle boundaries, resulting in subgrain separation. With the accumulation of strain, subgrains exhibit rotation, and dislocations continue to accumulate, causing columnar grains to gradually refine into equiaxed grains.

The rapid cooling and heating process of laser cladding induces significant temperature gradient differences, leading to solidification time delays, uneven element diffusion, uneven convective mass transfer in the melt pool,

and the presence of defects such as element segregation, pores, and cracks in the cladding layer, which reduce the performance of the cladding layer [32]. After ultrasonic vibration is introduced, the circulating, laminar, and turbulent flows generated by cavitation effects, acoustic streaming effects, and mechanical effects result in thorough stirring of the melt pool, reducing macroscopic segregation of the cladding layer and homogenizing the coating composition. Research conducted by Lv et al. [33] shows that the introduction of ultrasonic vibration during the laser cladding process reduces the aggregation of metal particles. As shown in Figure 3, due to the density difference between WC ( $15.55 \text{ g/cm}^3$ ) and Ni-based (approximately  $8.90 \text{ g/cm}^3$ ) materials, convection in the melt pool is weak, preventing the suspension of WC particles, which become concentrated in the center and bottom of the melt pool. However, ultrasonic vibration enhances the fluidity of the molten metal and the dispersion of WC particles through cavitation, acoustic streaming, and mechanical stirring, while increasing the viscosity of the melt pool, shortening the solidification time, making the downward movement of particles more difficult, and causing the WC particles concentrated at the bottom of the coating to rise, resulting in a significant reduction in the porosity of the cladding layer.

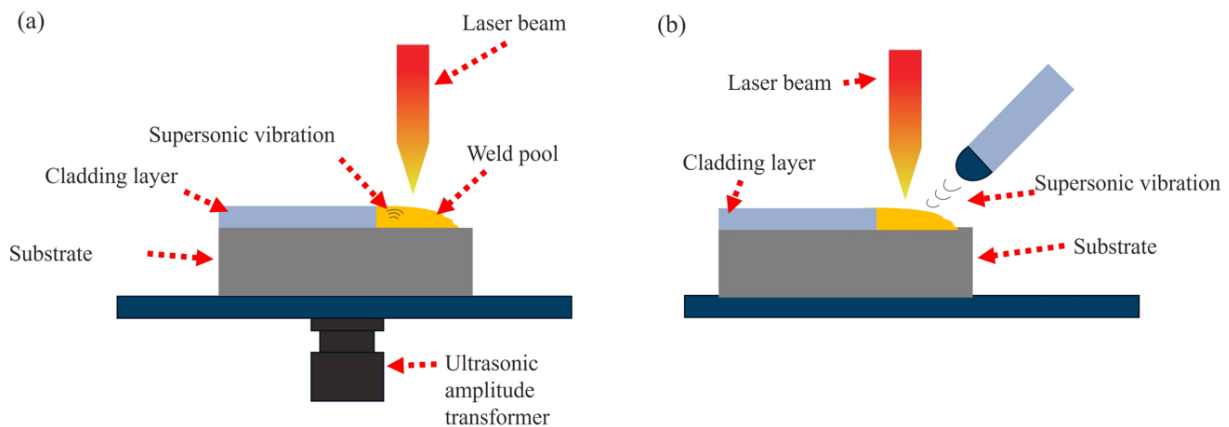


**Figure 1.** Ultrasonic vibration device application method, (a) contact type, (b) non-contact type

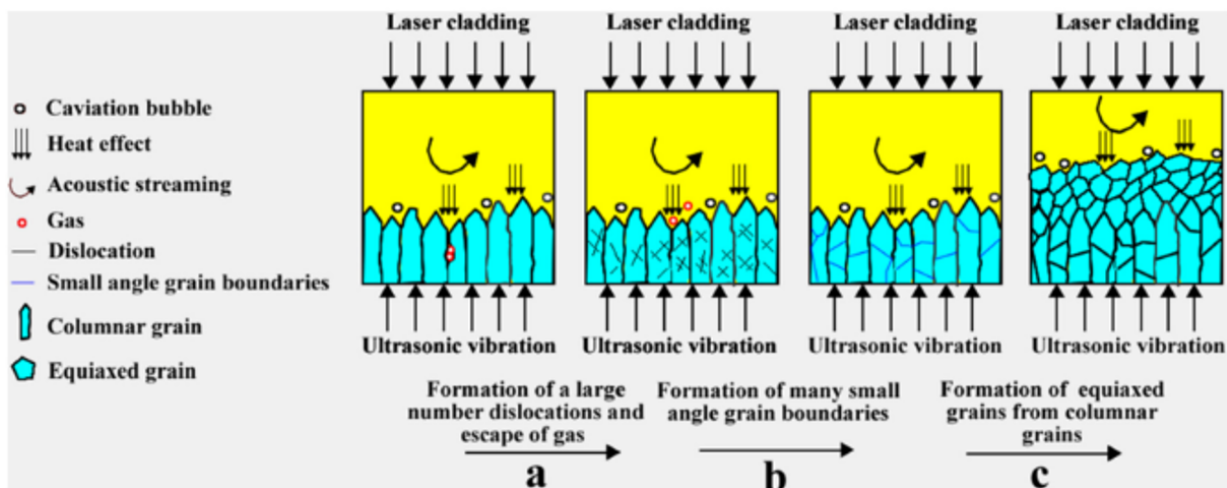


**Figure 2.** Schematic diagram of microstructure evolution in some primary columnar grains of ultrasonic-assisted laser cladding 316L stainless steel [31]

The problem of cracks has always been a focus of researchers during the laser cladding process. When a high-power laser beam is irradiated onto a metal surface, the energy of the laser is absorbed by the metal and converted into thermal energy. In a short time, the thermal energy is concentrated on the surface of the cladding area, forming thermal stress. When this exceeds the material's strength limit, cracks are formed [34]. Additionally, when the laser beam exits the scanning area, the cladding layer cools rapidly and is constrained by the surrounding cooler substrate, creating constraint stress. When the constraint stress exceeds the material's yield limit, microcracks appear on the surface of the cladding layer. The cavitation and mixing functions of ultrasonic vibration can improve the solidification state, reduce residual thermal stress, and decrease crack sensitivity [35, 36]. The study by Wang et al. [37] is also verified. Subgraphs (a)-(c) of Figure 4 show the coatings prepared on the surface of the IN718 alloy

substrate: IN718, IN718 + 50% WC, and ultrasonic vibration-assisted IN718 + 50% WC, respectively. As shown in subgraph (a) of Figure 4, during the laser cladding process, the protective gas and air are unable to escape the molten pool in time, resulting in the formation of porosities. In subgraph (b) of Figure 4, after WC is added to the molten pool, the convection is weakened, and hard particles are aggregated over a large area. Due to the differences in thermal expansion coefficients in different regions, transverse cracks are formed at the interface between the coating and the substrate. Longitudinal cracks, which extend preferentially along the dendrite growth direction, are observed in the laser overlap area, penetrating the entire cladding layer. The Marangoni effect is enhanced by ultrasonic waves through acoustic streaming and cavitation, promoting the flow inside the molten pool and reducing internal porosities. Furthermore, the carbides generated from the decomposition of WC under ultrasonic vibration increase the dynamic viscosity of the molten pool [36], improving the wettability and dispersion of the ceramic particles, increasing the degree of undercooling in the liquid phase, and promoting solid-phase nucleation. As a result, the microstructure is improved, and as shown in subgraph (c) of Figure 4, no significant crack defects are present in the coating. The ceramic iron-based composite coatings are prepared on the surface of 5CrNiMo steel by Zhang et al. [38]. Differences in hardness are found between the coatings with and without applied ultrasonic vibration, as shown in Figure 5. The surface morphologies of the two coatings are also significantly different; after the application of ultrasonic vibration, the number of metal nodules on the coating surface is noticeably reduced, resulting in a smoother appearance and decreased roughness. Figure 6 presents the average hardness and cross-sectional hardness of the coatings at different ultrasonic vibration powers. The ultrasonic stirring effect improves the flow field distribution in the molten pool, leading to a uniform distribution of ceramic reinforcement materials in the cladding layer, which results in increased and uniformly distributed hardness of the cladding layer.

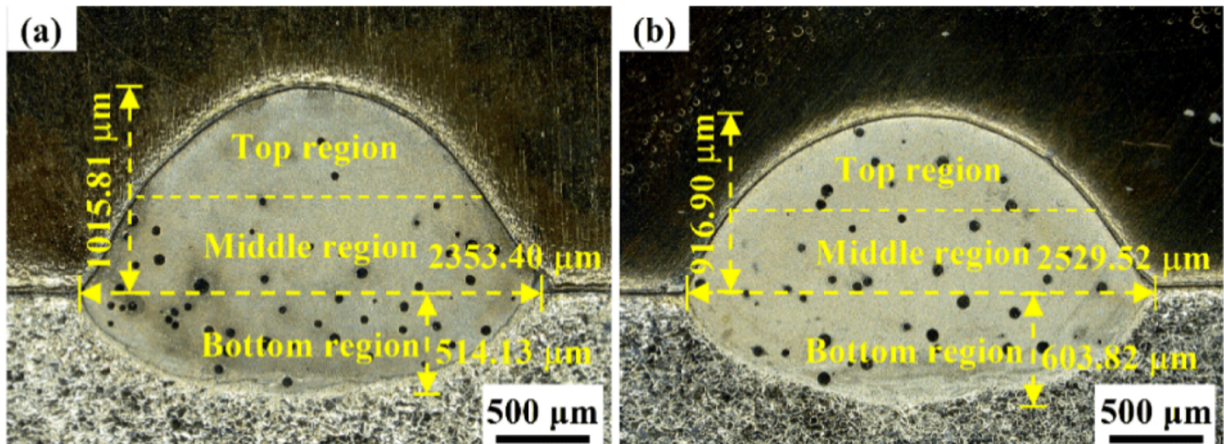


**Figure 3.** The typical cross-sectional morphologies of coatings: (a) without ultrasonic vibration; (b) with ultrasonic vibration [33]

In summary, ultrasonic vibration is widely utilized in laser cladding due to its advantages of simple equipment, no pollution, and low energy consumption. The introduction of ultrasonic vibration into laser cladding helps to address issues such as uneven microstructure, excessively large grains, and excessive residual stress in the as-cast microstructure.

## 2.2 Electromagnetic Ultrasonic Compound Field Assist

Most researchers focus on studying how a single electromagnetic field or ultrasonic field improves the performance of laser cladding layers. With advancements in materials technology, higher demands are placed on key components in the mechanical industry. Electromagnetic and ultrasonic fields have been coupled by some researchers to enhance laser cladding layers, in order to avoid the weakening effects that may arise from using a single auxiliary field [39]. Due to the limited range of ultrasonic vibration, optimal effects may not be achieved, and unexpected results are observed when an electromagnetic field is introduced.

Electromagnetic stirring is generated by the interaction of induced currents in the metal melt and the magnetic field, which creates electromagnetic forces. These electromagnetic stirring forces induce strong convection in the melt, facilitating melt flow and heat and mass transfer, achieving the ultimate goals of refining grains, reducing casting defects, decreasing composition segregation, and improving performance [40]. Hu et al. [41] observed that the electromagnetic field expanded the range of ultrasonic effects, significantly enhanced the nucleation of crystallization in the melt pool, and reduced temperature gradient differences, which had an important impact on grain size and morphology of the clad layer. The combined use of electromagnetic and ultrasonic fields effectively improves the

microstructure distribution and mechanical properties of the laser cladding layer, enhancing wear resistance and avoiding the occurrence of pores and cracks. As shown in Figure 7, Zhang et al. [42] addressed the high porosity issue in laser cladding layers and found that without auxiliary fields, the porosity reached 0.86% due to high solidification rates and resistance in the melt pool; however, under the combined action of ultrasonic vibration and electromagnetic fields, the Lorentz force induced by the electromagnetic field not only increased the escape velocity of pores but also enhanced cavitation effects and ultrasonic-induced effects, further strengthening Marangoni convection, significantly reducing large pores and lowering porosity to 0.118%. As shown in Figure 8, Zhou et al. [43] prepared Ni60A laser cladding layers with electromagnetic and ultrasonic composite fields, which promoted liquid metal flow, further eroded semi-solid and columnar grains, increased nucleation rates, and transformed the solidification of the melt pool from gradual to volumetric, refining the microstructure at the coating bottom. High-temperature liquid flow reduced cooling of the solid-liquid phases, promoted uniform element distribution, and optimized the coating's tribological and anti-corrosion properties. Under multi-physical fields, the number of cracks in the coating decreased by 76.92%, the average microhardness increased by 37.89%, the average friction coefficient decreased by 61.96%, the average wear loss decreased by 61.05%, and the corrosion rate decreased by 93.01%.

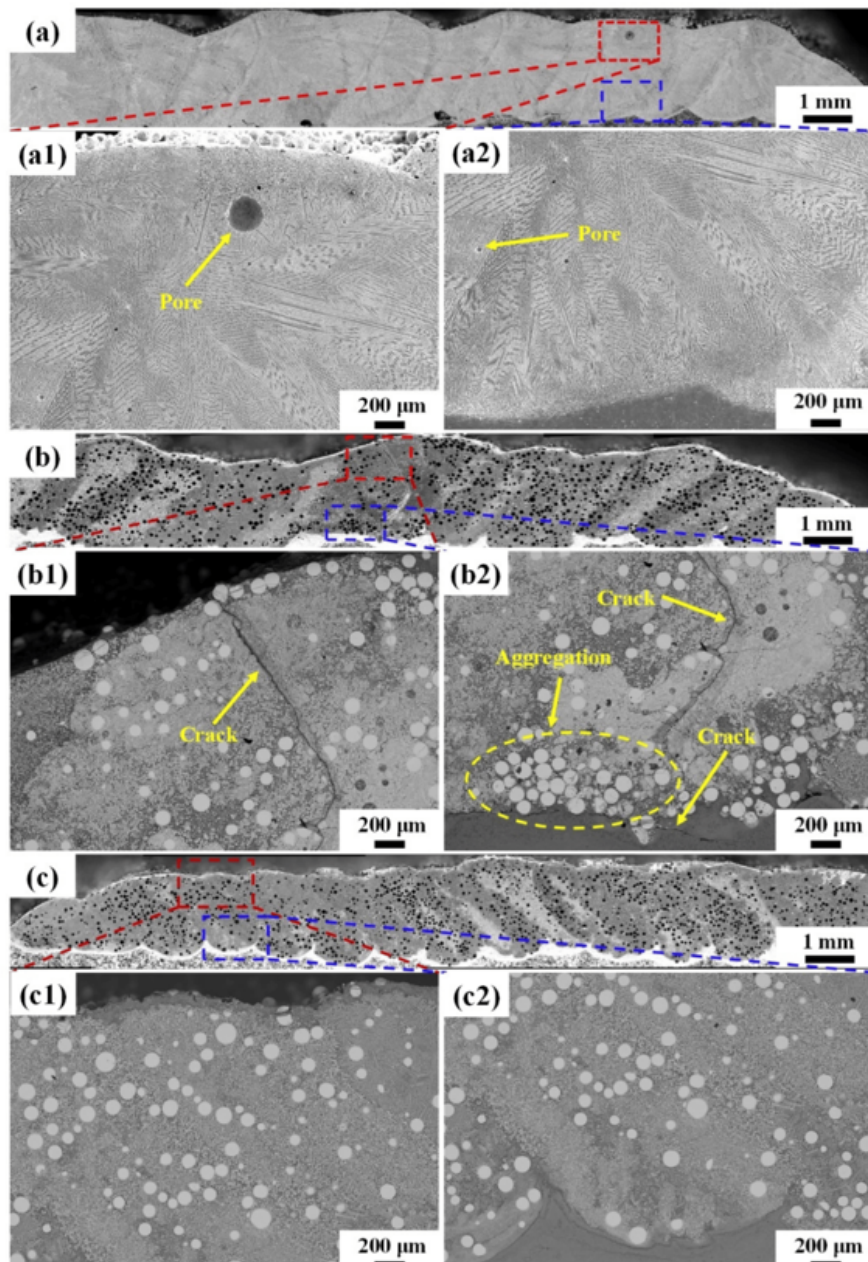


**Figure 4.** Cross-sectional morphologies of different coatings: (a) Coating A; (b) Coating B; (c) Coating C; (c1) and (c2) represent partial enlarged images of the top and bottom regions respectively [37]

In summary, the introduction of electromagnetic forces and ultrasonic fields intensifies the convective effects in the melt pool and suppresses element segregation, resulting in grain refinement. Under the combined fields, coatings with dense microstructures, low element segregation, and good mechanical properties can be obtained.

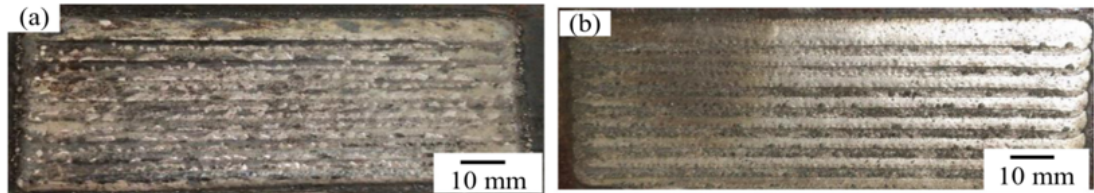


**Figure 5.** Typical top view of the macro-appearance of the coatings: (a) without ultrasonic vibration; (b) with 200 W ultrasonic vibration [38]

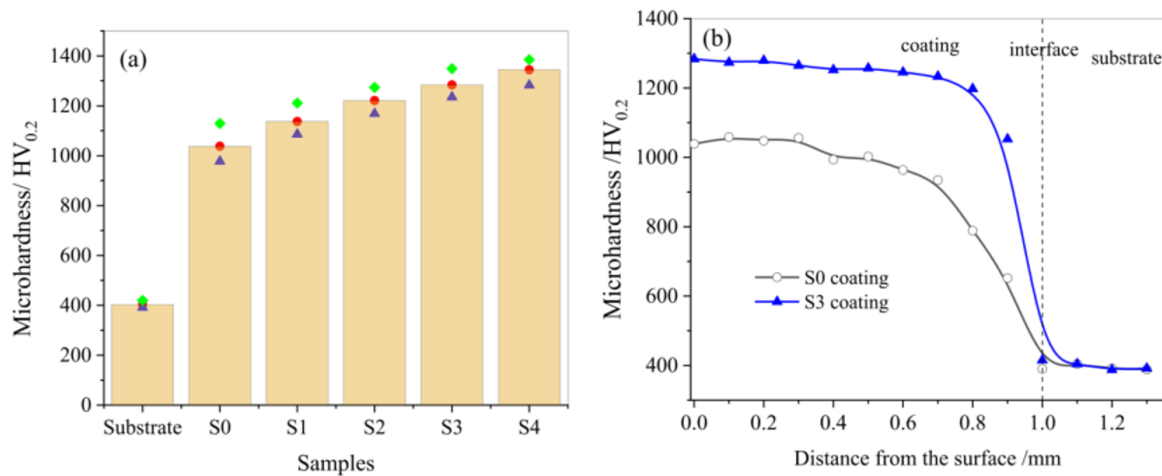


**Figure 6.** Micro-hardness of the substrate and coatings: (a) average hardness; (b) typical micro-hardness distribution along the depth of the coatings [38]

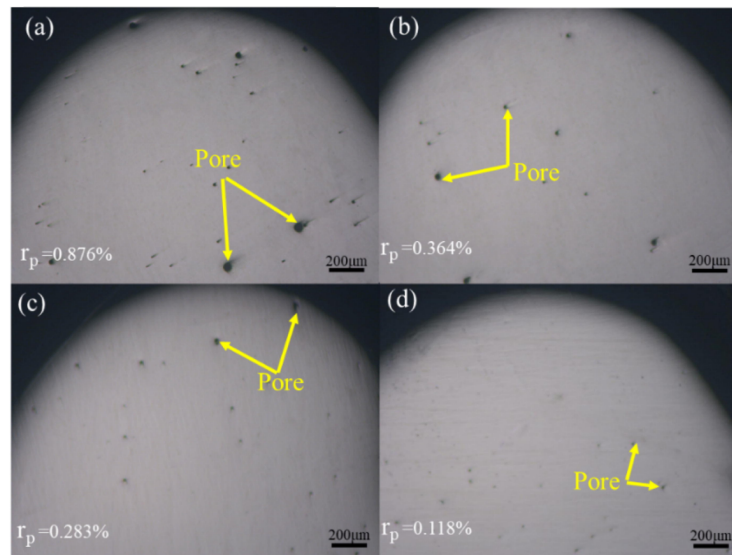


**Figure 7.** The morphologies of the coating fabricated by laser cladding assisted without and with different external physics field: (a) without field; (b) ultrasonic field; (c) electromagnetic field; (d) hybrid ultrasonic and electromagnetic field [42]

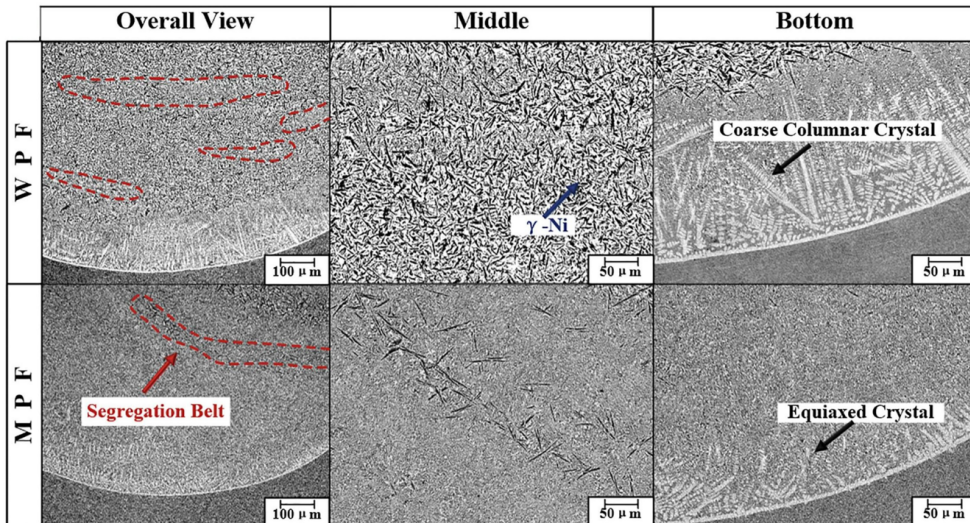


**Figure 8.** Microstructure of Coating: without physical fields (WPF), magnetic field, electric field, ultrasonic field (WPF) [43]

### 3 Ultrasonic Rolling

#### 3.1 Ultrasonic Rolling Technology

Ultrasonic rolling technology combines traditional rolling processes with ultrasonic techniques. Through ultrasonic impact energy and ball pressing on the workpiece surface, a gradient structure is formed on the metal surface. This structure effectively avoids local stress concentration and allows the metal to exhibit good plasticity with increasing strength [44]. After ultrasonic rolling treatment, the surface grain of the workpiece is significantly refined, and residual compressive stress is introduced, thus improving mechanical properties, fatigue resistance, and corrosion resistance [45]. A typical example is that the residual compressive stress generated in the near-surface region of the metal during processing can offset the tensile stress applied to the surface, delaying the formation of surface cracks; the residual compressive stress in the near-surface region of metal parts during corrosion can also mitigate surface pitting and crack propagation [46]. Xu et al. [47] enhanced the corrosion resistance of laser additive manufactured 316L stainless steel surfaces using ultrasonic rolling technology. By increasing the static pressure of ultrasonic rolling, the degree of plastic deformation of the coating is intensified, dislocations and grain boundaries are increased, grain refinement occurs, and surface roughness is improved. In a corrosive environment, the rough surface with high-density defects more readily transmits electrons, exhibiting a higher corrosion rate, and due to easier electron release, protrusions are more susceptible to corrosion than depressions. As shown in Figure 9, after ultrasonic rolling, a peak-to-valley effect occurs where protrusions are pressed into grooves. The residual compressive stress near the surface counteracts the tensile stress generated by  $\text{Cr}_2\text{O}_3$  growth, stabilizing the oxide film. The enhancement in corrosion resistance after ultrasonic rolling is mainly due to the combined effects of improved surface roughness, grain refinement, increased  $\text{Cr}_2\text{O}_3$  content in the passivation film, work hardening, and residual compressive stress.

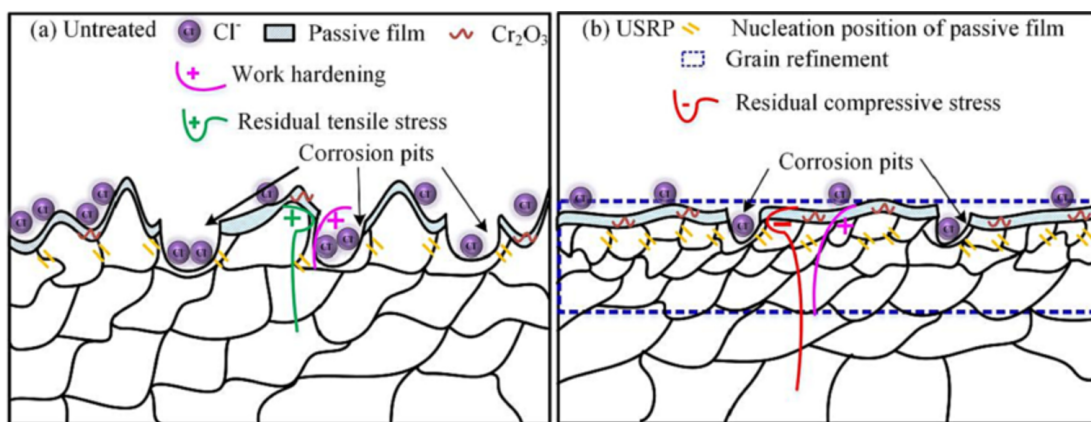


**Figure 9.** Schematics of corrosion progresses of sample: (a) turning sample; (b) USRP [47]

Ultrasonic rolling technology, as a post-processing technique, is used to reduce quality defects in coating formation, refine coating grains, decrease surface roughness, and produce deep residual compressive stresses while increasing surface hardness. These improvements significantly enhance the wear resistance, corrosion resistance, and fatigue resistance of laser cladding layers. However, single rolling reinforcement has certain limitations. When process parameters exceed the plastic deformation limit of the material, defects on the material surface, such as wrinkling and cracking, may increase, leading to localized fatigue damage and affecting the material's fatigue life. Additionally, for materials with high surface hardness, such as hard alloys, single rolling treatment is difficult to achieve deep reinforcement effects, leading to the development of ultrasonic rolling composite reinforcement processes.

### 3.2 Pulsed Current - Ultrasonic Rolling Technology

Pulsed current, as an advanced external magnetic field treatment technology for metallic materials, is used to influence their plasticity, recrystallization, phase transformation, casting microstructure, and fatigue life. In the plastic processing of metallic materials, the application of electrical pulses reduces deformation resistance. The impact vibration effects, thermal softening effects, and electroplastic effects produced by ultrasonic waves and electrical pulses significantly increase the plastic deformation of metals and introduce deeper gradient layers. Based on the acceleration of phase transformation, dislocation migration rates, and atomic diffusion mechanisms by electrical pulses, the processing hardening and number of defects in metallic materials are significantly reduced. Xie et al. [48] found that with the aid of pulsed current, metallic materials experience instantaneous high temperatures and electroplastic effects due to thermal and non-thermal effects. Instantaneous high temperatures reduce dislocation width, increase stacking fault energy, and make dislocations less likely to twin while having higher migration rates. The electro-pulsed ultrasonic rolling process (EP-USRP) demonstrates a different dislocation strengthening mechanism compared to ultrasonic rolling, while exhibiting superior comprehensive mechanical properties, with higher strength and maintained plasticity. Wang et al. [49] noted the impact of pulsed current density on the microstructure of the workpiece surface. As shown in Figure 10, compared to turning, the microstructure of samples treated with ultrasonic rolling changes, but microcracks and defects still exist, which may potentially become crack sources and negatively impact the fatigue life of mechanical components. As pulsed current density increases, the joule heating effect of the pulsed current raises the surface temperature of the samples. The pulsed current density is proportional to the surface equilibrium temperature, and a trend of crack healing on the workpiece surface is observed. When the pulsed current density reaches a certain value ( $1.34 \text{ Amm}^{-2}$ ), surface cracks and defects in EP-USRP treated samples are nearly eliminated. Sun et al. [50] observed that pulsed current frequency is also an important factor affecting the surface properties of workpieces. As shown in Figure 11, comparisons between turning, ultrasonic rolling, and electro-pulsed ultrasonic rolling with different pulsed frequencies reveal that EP-USRP with an appropriate frequency (400 Hz) significantly improves the microhardness and nanoindentation hardness of alloys, with further improvements in surface quality and wear resistance. The coupling of thermal and non-thermal effects significantly increases dislocation migration rates and stacking fault energy, maintaining a new balance between electro-pulsed softening effects and ultrasonic rolling processing hardening effects, which is beneficial for further grain refinement and increasing the depth of the strengthened layer. Sun et al. [51] applied the EP-USRP treatment to the surface of nickel-aluminum bronze alloys and observed grain refinement on the surface, with hardness affecting a depth greater than  $1000 \mu\text{m}$ . After corrosion, USRP-treated samples exhibit larger cavitation pits on the surface. With the introduction of pulsed current, significant resistance differences between the matrix phase and precipitated phase create localized high temperatures at phase interfaces, which can alleviate bonding issues to some extent, and the surface of EP-USRP-treated samples does not show large cavitation pits.

In summary, under the influence of pulsed current, the electro-plastic effect accelerates dislocation movement and untangles dislocation entanglements, expanding the grain refinement region and residual stress depth in ultrasonic rolling. The thermal effects of the pulsed current alleviate issues such as plastic deformation difficulties caused by material work hardening, improving surface integrity, and enhancing various surface properties.

### 3.3 Temperature Field Assisted Ultrasonic Rolling Technology

Temperature-field-assisted ultrasonic rolling is also a common method. High-strength alloy powders are typically used as coating materials in laser cladding. Due to the high hardness and relatively low plasticity of these materials, applying temperature-field-assisted ultrasonic rolling can further enhance the plastic deformation of high-hardness materials and promote the healing of microcracks [52]. As the temperature increases, the depth of the surface hardening layer and residual compressive stress under ultrasonic rolling also increase [53]. However, excessively high temperatures can lead to a reduction in the surface strain energy, increasing the dislocation migration energy, and making the material more likely to transition to an equilibrium state. As shown in Figure 12, Shen et al. [54] utilized the property of metals to flow easily at high temperatures and heated laser-clad iron-based coating samples using a heating coil to a certain temperature. Figure 13 shows the microstructure of samples at different temperatures and at different times. At  $100^\circ\text{C}$ , pores and microcracks are still present on the coating surface. In contrast, at  $250^\circ\text{C}$  and

400°C, no significant microcracks are observed on the coating surface, indicating that within the experimental range, higher heating temperatures result in better surface smoothness, reduced roughness and porosity, smaller grain size, increased hardness, and greater residual compressive stress. Zhang et al. [55] observed that under ultrasonic thermal rolling, the coating absorbs sufficient heat to soften, the atomic spacing increases, and the metal bonds become weaker and break more easily, leading to enhanced plastic deformation. As shown in Figure 14, micro-peaks of the coating are compressed and flowed, with the flowing material filling the pits, eliminating surface cracks. Internal cracks are bridged under plastic flow, suppressing large-scale crack propagation and surface cracking, while surface roughness varies with different pressing depths. Luan et al. [56] observed that within the temperature range of 150°C to 200°C, the surface smoothness of workpieces processed by ultrasonic rolling is optimal. The thermal softening effect of the material plays a positive role by enhancing deformation strengthening effects without changing the material's microstructure. Under the combined action of ultrasonic vibration and thermal field effects, the material undergoes work hardening, age hardening, and precipitation hardening, with the maximum residual stress amplitude and influence layer depth being achieved.

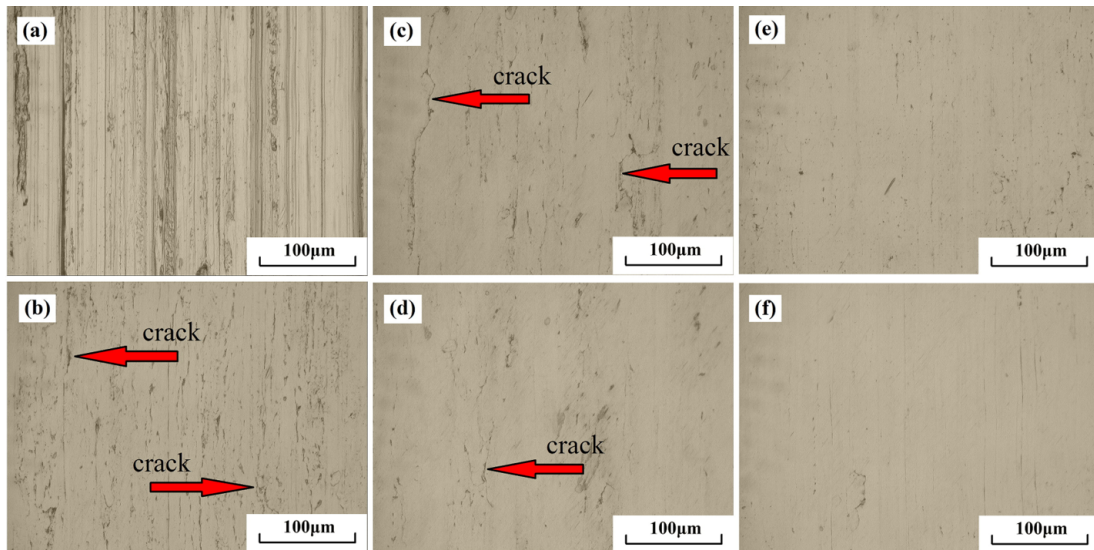


**Figure 10.** (a) The micro-morphology evolution on specimen surfaces which treated by turning; (b) USRP; (c) EP-USRP with different pulse current density  $0.62\text{Amm}^{-2}$ ; (d)  $0.91\text{Amm}^{-2}$ ; (e)  $1.12\text{Amm}^{-2}$ ; (f)  $1.34\text{Amm}^{-2}$  [49]

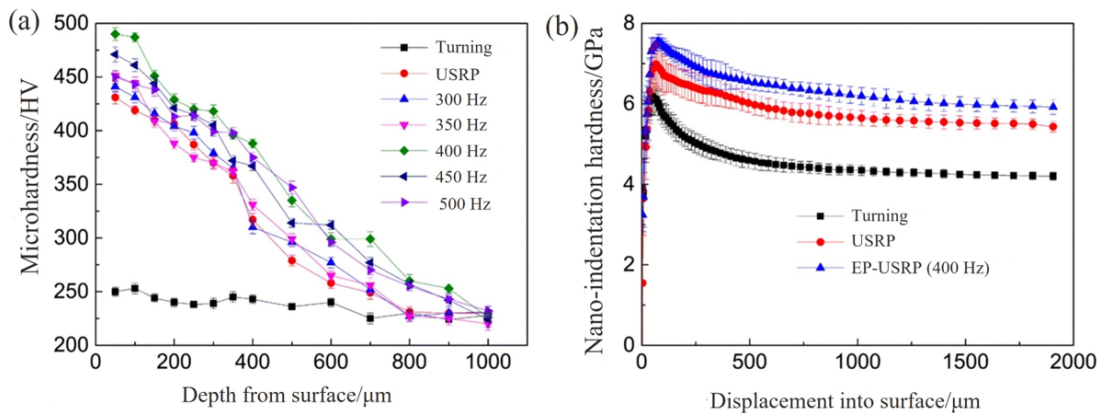


**Figure 11.** The hardness distribution within the strengthened layer: (a) Vickers microhardness; (b) nanoindentation hardness at 50 µm below the surface [50]

Compared to ultrasonic rolling, temperature field-assisted ultrasonic rolling introduces an appropriate temperature that promotes the healing of fine cracks within the coating. This method not only excels in achieving fine microstructures but also enhances the depth of residual compressive stress and work hardening layers. At the same time, the ability of the sample surface to resist plastic deformation is slightly reduced, which helps improve the surface smoothness of the laser cladding layer.

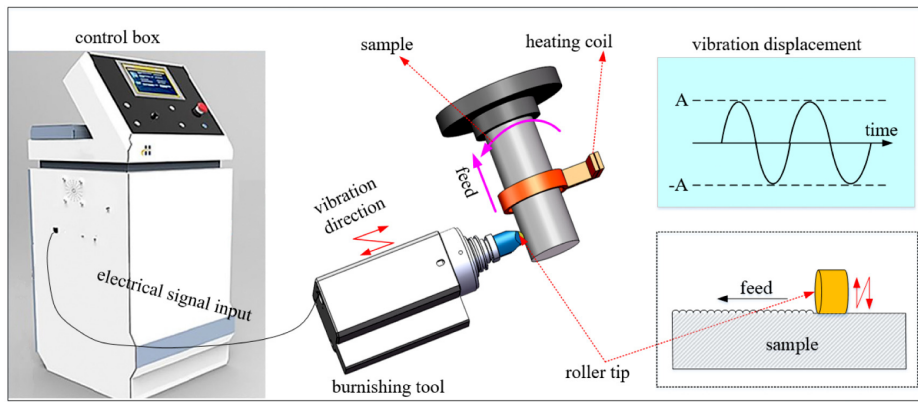


**Figure 12.** Illustration of UWB/HT treatment [54]

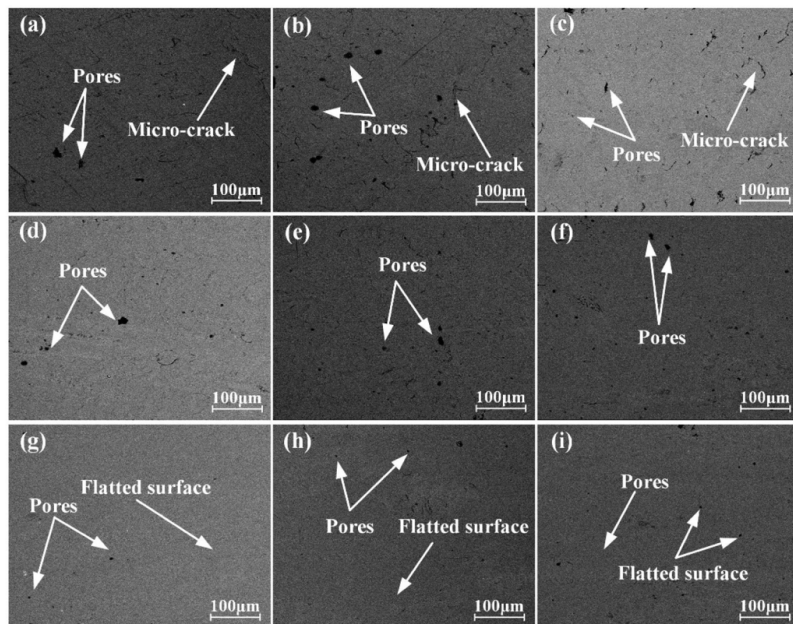


**Figure 13.** Surface morphologies of the UWB/HT-treated samples: (a)-(c)  $100^{\circ}\text{C} + 0.5/1/2 \text{ h}$ ; (d)-(f)  $250^{\circ}\text{C} + 0.5/1/2 \text{ h}$ ; (g)-(i)  $400^{\circ}\text{C} + 0.5/1/2 \text{ h}$  [54]

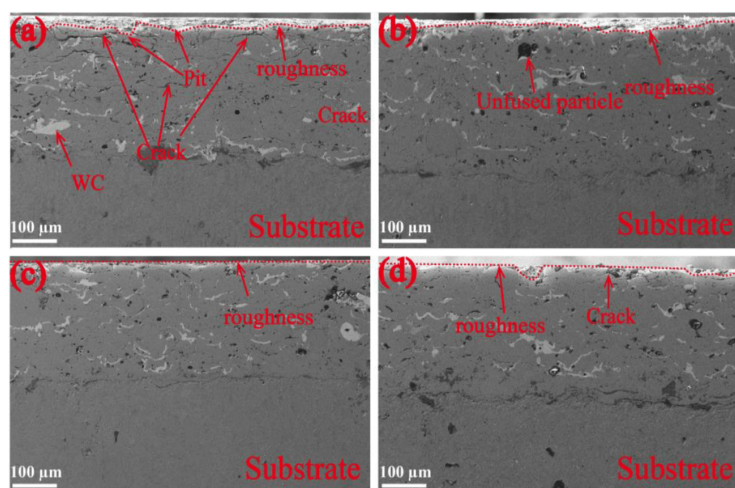


**Figure 14.** The structure of different preloading depths: (a) Untreated; (b) HT + UDR + 0.20 mm; (c) HT + UDR + 0.25 mm; (d) HT + UDR + 0.30 mm [55]

## 4 Ultrasonic Impact Treatment Technology

Ultrasonic impact treatment (UIT), as a novel cold processing surface treatment technology, is characterized by its point contact method, high strain rate, and high energy density input. Utilizing the cold shrinkage characteristics of metals at room temperature, plastic deformation is generated on the surface through high-frequency impacts with strain rates of  $10^3 \sim 10^4 \text{ s}^{-1}$ . This results in the formation of a thick impact deformation hardening layer within a short period, causing lattice distortion, dislocation multiplication, and slip sliding. UIT uses high-power ultrasonic waves to convert electrical energy into high-frequency amplitude through a transducer, and this amplitude is then amplified by a sonotrode to drive impact needles onto the surface of the workpiece. Under the combined effect of high-frequency impacts and ultrasonic oscillations, severe plastic deformation is induced on the surface of the laser cladding layer, resulting in high hardness, high compressive residual stress, as well as finer grain structure and reduced surface roughness. This significantly enhances the strength, reliability, and durability of the laser cladding layer [57].

### 4.1 Refinement of Microstructure

One of the key advantages of UIT in enhancing laser cladding coatings is the improvement of the microstructure. During ultrasonic impact, repeated external loads applied to the material surface significantly induce plastic deformation, which leads to the generation of dislocations and the introduction of non-equilibrium defects. Under the combined effect of plastic deformation and ultrasonic oscillations, high-density dislocations in localized areas become entangled, and after reaching a certain extent, they rearrange to reduce energy configuration, forming dislocation walls that eventually evolve into nanocrystals. UIT disrupts the original coarse grain structure, forming a more uniform and refined grain structure. These fragmented and refined grains provide more nucleation sites during subsequent deposition, thereby promoting grain refinement. Wang and Shi [58] found that severe plastic deformation is generated on the surface and near-surface of metal components by ultrasonic impact, with mechanical twinning and dynamic recrystallization playing a key role in refining the microstructure. Wang et al. [59] discovered that after increasing the amplitude of ultrasonic impact, as shown in Figure 15, significant plastic deformation could be observed on the top of the coating after UIT treatment, with the depth of the deformed layer increasing gradually with the amplitude. The as-deposited coating without impact treatment contains almost no low-angle grain boundaries, while increasing the amplitude leads to more low-angle grain boundaries at the top of the coating. At this point, the thickness of the ultrasonic impact-affected layer is about  $100\text{-}400 \mu\text{m}$ , and the grain size is  $64.067 \mu\text{m}$  when the amplitude is  $20 \mu\text{m}$ , which is approximately 34% of the original size. During the impact process, dislocation pile-ups hinder dislocation movement, resulting in improved mechanical properties of the sample. It is observed by Zhang et al. [60] that a large number of randomly distributed elongated structures are present on the surface of the AlCoCrCuFeNi high-entropy alloy after UIT treatment (subgraph (b) of Figure 16). The grain refinement is clearly indicated in the subgraph (d) of Figure 16 Inverse Pole Figure (IPF) maps, showing the presence of many nanocrystals within the elongated structures. The average grain size is refined from  $34.4 \mu\text{m}$  to  $18.6 \mu\text{m}$ . Song et al. [61] classify the cladding layer into the impact-affected zone (I), the impact-transition zone (II), and the unaffected zone (III) based on the degree of grain refinement after UIT. Subgraphs (a) and (d) of Figure 17 show that with increasing depth, a significant number of grain boundaries are observed in regions I and II of the cladding layer after UIT treatment, further verifying the grain refinement and exhibiting features similar to a gradient structure. Subgraphs (b) and (e) of Figure 17 show the KAM (Kernel Average Misorientation) distribution calculated by EBSD. Severe plastic deformation occurs at the top of the cladding layer after UIT, with higher KAM values primarily located at the top of the cladding layer. As the depth increases, the KAM values gradually decrease. Current research indicates that the density of geometrically necessary dislocations (GNDs) is positively correlated with KAM values. The role of GNDs is to accommodate non-uniform micro-deformation and maintain continuity, and GNDs can be represented by the following Eq. (1) [61]:

$$\rho_{GND} = \frac{2\theta_{KAM}}{ub} \quad (1)$$

where,  $\theta_{KAM}$  is the average local misorientation,  $b$  is the Burgers vector, and  $u$  is the unit length (step size used in EBSD characterization). Subgraphs (c) and (f) of Figure 17 show that after UIT treatment, the number of LAGBs in the coating increases, with a particularly notable increase in Region I. Region I has a higher dislocation density and a higher degree of plastic deformation. During deformation, high strain induces favorable dislocations to move preferentially. As the degree of deformation increases, dislocation pile-ups and entanglements form dislocation walls and sub-grains.

### 4.2 Adjustment of Surface Stress Distribution

One significant effect induced by UIT is the reorganization of stress states and the introduction of residual compressive stress, which helps to enhance the overall performance of the components. Damage to the parts primarily arises from tensile residual stresses, which reduce the corrosion resistance, fracture toughness, and fatigue life of the parts, while appropriate compressive stress helps to inhibit crack formation, thereby extending the fatigue life of the

components [62, 63]. During the laser cladding heating and cooling processes, temperature gradients exist within the material, and uneven thermal expansion and contraction generate thermal stresses. Zhang et al. [64] combined selective laser melting with UIT technology in the Ti6Al4V alloy, where UIT treatment reduced the residual tensile stress from 176.3 MPa to 49.9 MPa, and defects in the cladding layer were also hammered flat or even eliminated. Hua et al. [65] demonstrated that hard particles affect the stress state in UIT-treated areas. In Figure 18, UIT treatment of laser-clad TC4/Ti2AlC/B composite coatings showed that with 3 wt%, 6 wt%, and 9 wt% B content, residual stresses decreased by 79 MPa, 71 MPa, and 64 MPa, respectively. UIT can produce significant compressive plastic deformation on the coating surface, squeezing the grains, generating certain residual compressive stresses in both the coating surface and interior. At high strain rates, dislocation walls and entanglements increase, grains are fragmented and refined, and stress is stored within the grains. When B content is high, a large amount of hard phase forms inside the coating, increasing surface hardness, making it difficult for UIT to produce significant compressive plastic deformation, resulting in relatively small changes in the original stress values.

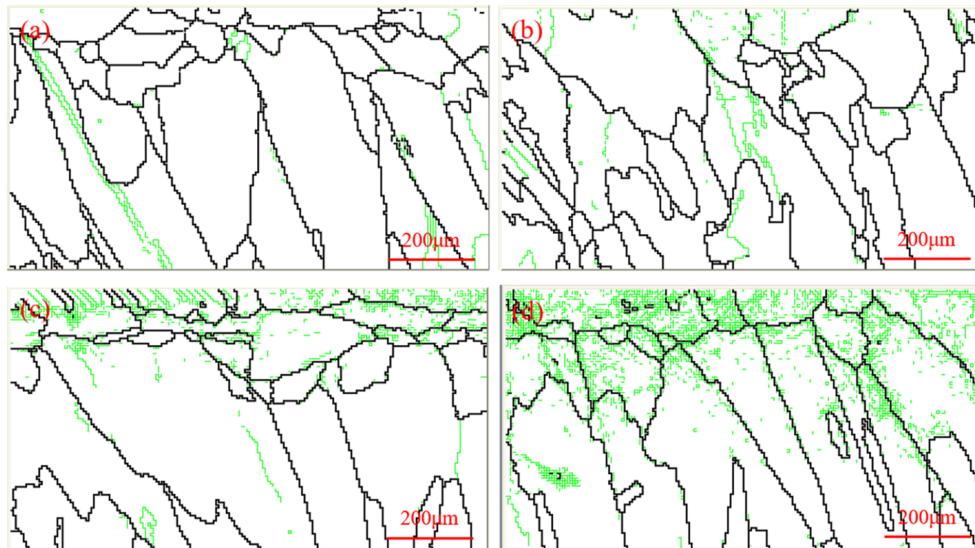


**Figure 15.** Cross-sectional morphology of CrCoNi coatings impact layer under different impact amplitudes: (a) 0 $\mu\text{m}$ ; (b) 10 $\mu\text{m}$ ; (c) 15 $\mu\text{m}$ ; (d) 20 $\mu\text{m}$  [59]

#### 4.3 Improvement of the Overall Performance of the Cladding Layer

Part of the failure of mechanical components is caused by surface wear of the material. The plastic flow induced by ultrasonic impact can induce an effect of filling the valleys with peaks, significantly reducing surface roughness. With a decrease in the grain size and roughness of the surface layer, a gradient structure is formed downwards along the impact surface, with higher hardness closer to the surface. This has also been demonstrated in Li et al. [66] research. As shown in Figure 19, ultrasonic impact treatment reduces the surface roughness of Al<sub>x</sub>CoCrFeMnNi high-entropy alloys, while the microstructure becomes finer. The refined microstructure and precipitation strengthening mechanisms further increase surface hardness [67], generating a work-hardening effect, with the highest microhardness in the surface layer [68], and greatly improved wear resistance. Zhang et al. [69] found that the microhardness of the Ti40 cladding layer treated by UIT increased by 43.5% (531 HV), and the microhardness of the sample gradually decreased in the normal direction. The trend of microhardness changes in the Ti40 cladding layer after UIT conforms to the Hall-Petch formula. According to the Hall-Petch formula [70, 71], which indicates that the smaller the grain size, the higher the material hardness, the fine-grain strengthening and work-hardening effects induced by UIT significantly improve the hardness of the cladding layer.

$$H_V = H_0 + Kd^{-\frac{1}{2}} \quad (2)$$

In the formula,  $H_V$  is the hardness value, and  $H_0$  and  $K$  are constants;  $d$  is the average grain size. The changes in surface microstructure, surface hardness, residual stress, and surface roughness induced by ultrasonic impact are further enhancing the corrosion resistance of the modified surface. UIT treatment is applied to iron-based coatings prepared by high-speed laser cladding by Zhang et al. [72]. Due to the decrease in roughness and refinement of surface grains, corrosion ions are less likely to accumulate on the coating surface, which favors the formation and presence of a passivation film, thereby improving corrosion resistance [73]. Li et al. [74] found that significant precipitates are present in the laser-clad Al0.5CoCrFeMnNi high-entropy alloy coatings. As shown in Figure 20, precipitates

at grain boundaries act as corrosion sources in the corrosive medium, causing surrounding areas to corrode and form corrosion pits. Long-term exposure to corrosive liquids leads to the formation of corrosion channels along continuous precipitates at grain boundaries, resulting in corrosion failure. After UIT, fine grains are formed on the surface, precipitates at grain boundaries develop cracks and fine particles. Under the high strain rate of ultrasonic impact, the plastic deformation of the matrix reduces the grain boundary gaps, decreasing the corrosion rate and significantly reducing the size and number of corrosion pits.

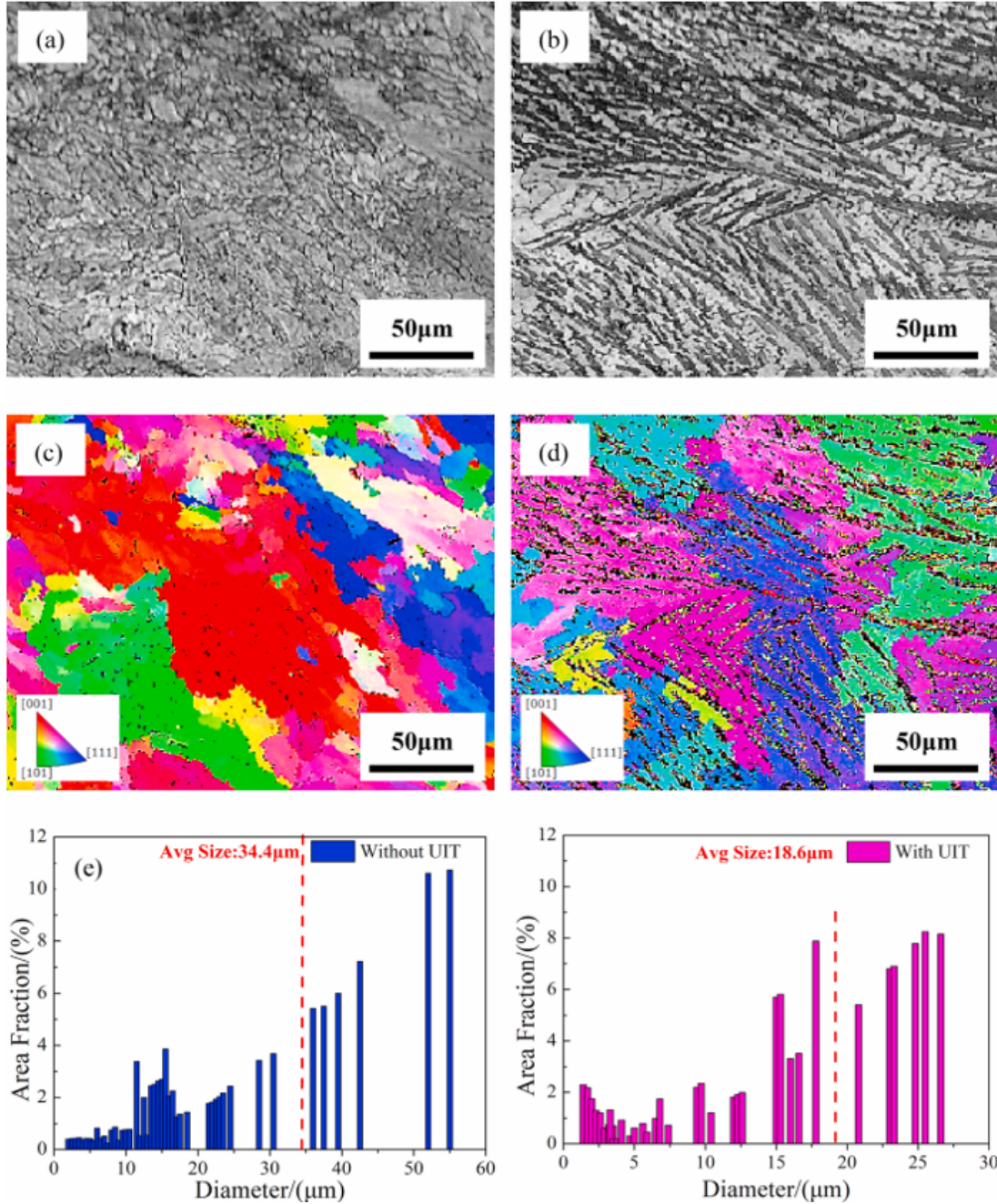


**Figure 16.** AlCoCrCuFeNi HEA coatings: (a), (c), (e) without UIT; (b), (d), (f) UIT [60]

Fatigue cracks are initiated from the material surface or internal regions, with microscopic cracks, stress concentration areas on the material surface, and microstructural defects within the material being susceptible to fatigue crack initiation. The compressive residual stress induced by surface plastic deformation after ultrasonic impact provides crack-closing stress and resistance to plastic deformation at the crack tip, enhancing the material's fatigue performance. In the study by Dekhtyar et al. [75], UIT results in lower surface roughness and compressive residual stress within the surface deformation layer, which reduces the initial crack propagation rate [76], significantly improving the material's fatigue strength and service life. Eremin et al. [77] conducted ultrasonic impact strengthening

on Ti-6Al-4V prepared by selective laser melting, finding that fatigue strength increased by approximately 60% after UIT treatment. Walker et al. [78] performed UIT on TC4 prepared by direct metal laser sintering (DMLS), as shown in Figure 21, and observed a 200% increase in fatigue life under 400 MPa loading stress after UIT treatment.

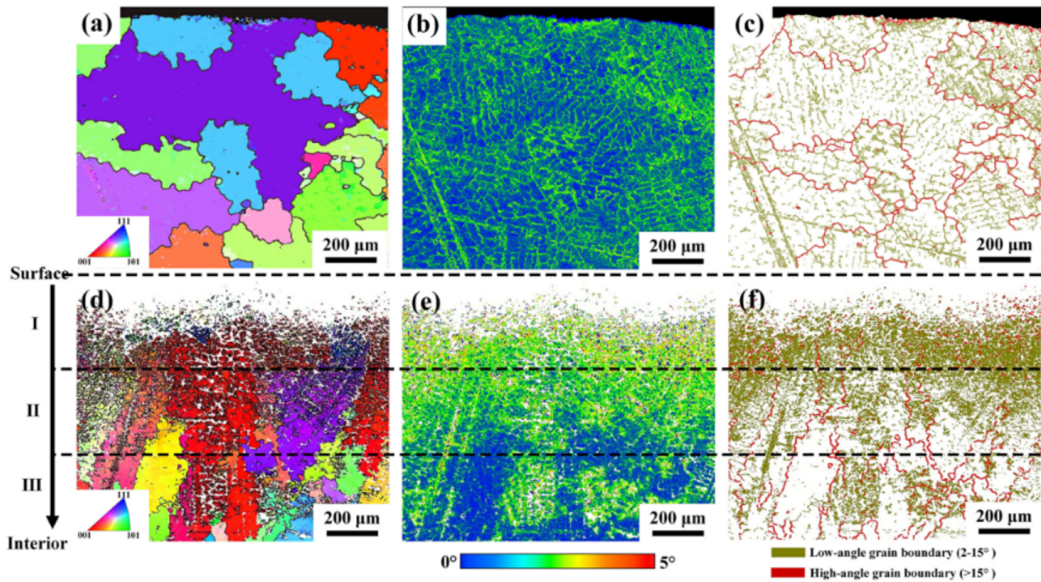


**Figure 17.** EBSD analysis of cross-section of HEA: (a), (d) IPF maps of HEA before and after UIT; (b), (e) KAM map of HEA before and after UIT; (c), (f) Misorientation angles distribution map of HEA before and after UIT [61]

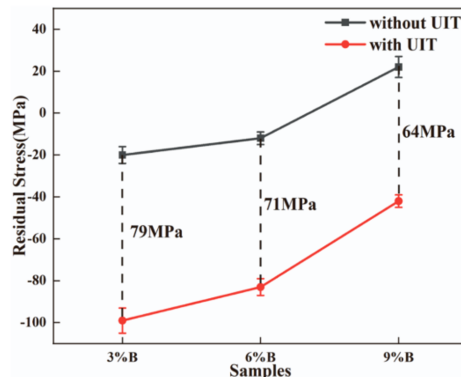


**Figure 18.** Residual stresses inside the coating with or without ultrasonic impact treatment with different B contents [65]

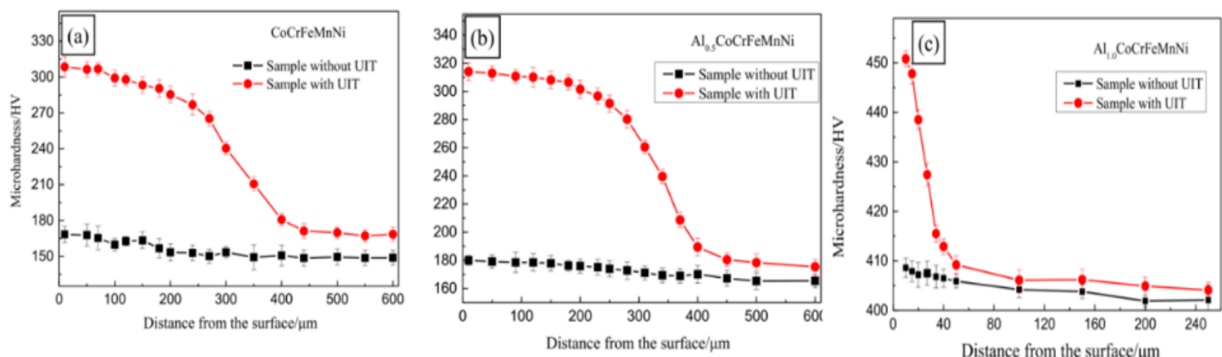


**Figure 19.** Microhardness curves of  $\text{Al}_x\text{CoCrFeMnNi}$  HEA samples by ultrasonic impact treatment using Vickers microhardness tester [66]

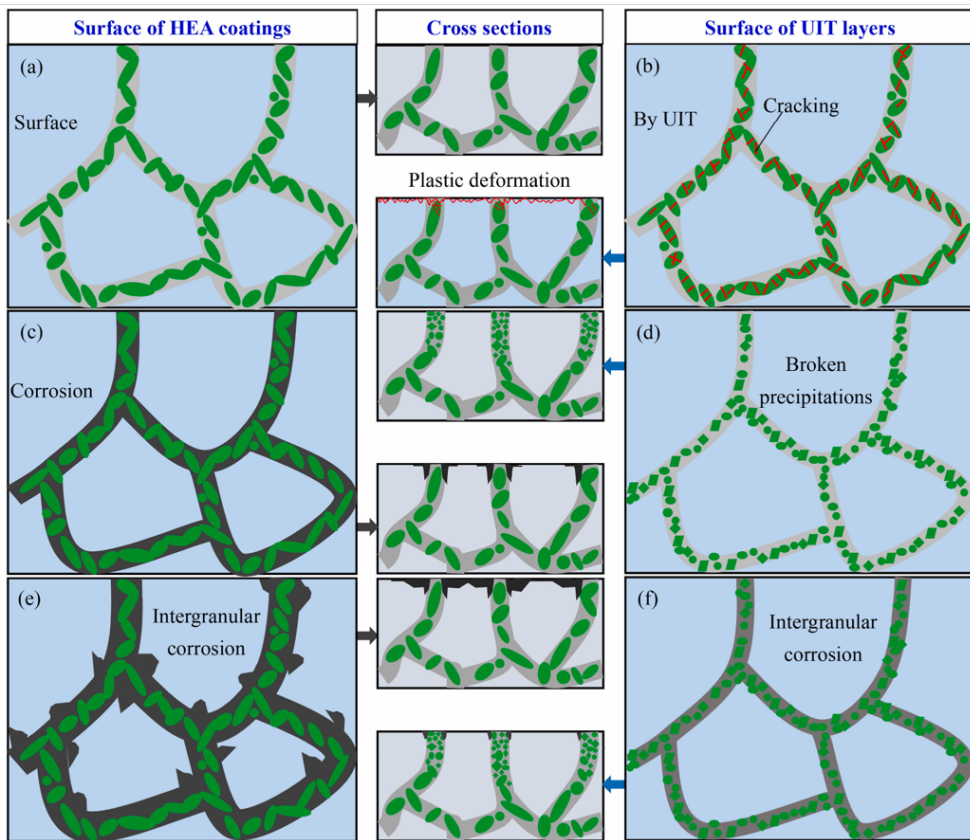


**Figure 20.** Schematic diagram of comparison between Al0.5CoCrFeMnNi cladding coating and impacted layer: (a) Surface of laser cladding coating; (b) treated by UIT; (c) corrosion occurrence on the surface of cladding coating; (d) broken precipitations and narrowed grain boundaries; (e) extensive intergranular corrosion; (f) slight intergranular corrosion [74]

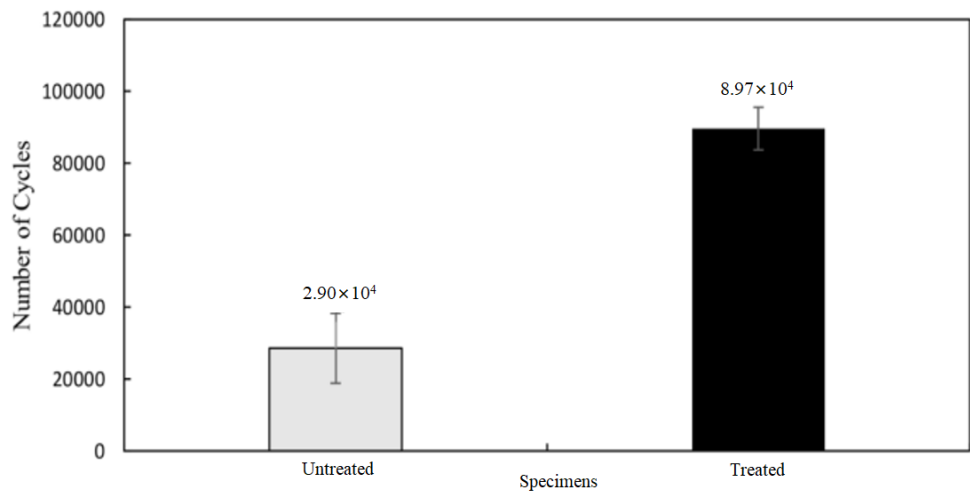


**Figure 21.** Average fatigue life of treated and untreated Ti-6Al-4V specimens tested at 400 MPa [78]

Overall, after UIT, defects and roughness of the coating layer are significantly reduced, and a smoother surface decreases stress concentration in the workpiece. Additionally, after impact, the original structure in the surface deformation layer of the coating is fragmented into fine grains, which increases the microhardness of this region, suppresses the initiation and propagation of associated cracks, and contributes to extending the service life of the components.

## 5 Conclusion and Prospect

The introduction of ultrasonic strengthening technology effectively reduces defects present in the laser-coated layer, and enhances the overall strength of components by regulating microstructure, residual stress, and mechanical properties. This has significant practical implications for strengthening high-performance critical components. However, there are few specialized researchers in this field, and the mechanisms by which ultrasound affects material wear resistance, corrosion resistance, fatigue performance, and microstructure are not sufficiently explored, limiting a comprehensive understanding of the impact of process parameters on component performance. Currently, ultrasonic strengthening technology still faces the following issues in laser cladding technology:

1. Mainstream research is focused on large metal materials, and there is less investigation into the surfaces of small precision components and non-metal materials. Strengthening is often performed in disordered environments, with low machine precision and a lack of online monitoring systems.

2. The strengthening mechanisms between ultrasonic strengthening and laser cladding need to be explored in depth. Since the effect time of ultrasonic strengthening is short, mainstream research is mainly comparative and has not fully explained the enhancement effects after the introduction of ultrasound. The impact of ultrasonic strengthening process parameters on the surface performance and fatigue life of laser-clad components requires further study, and there is a lack of relevant simulation analysis.

3. Currently, the ultrasonic-enhanced composite process is mostly stayed at the research and experimental stage, and high application costs prevent mutual cooperation between industry, academia, and research.

Future research should delve into the application of ultrasonic-enhanced technology in additive manufacturing, addressing surface defects and stress issues. Investment in the development of Mordyukomposite technologies, processes, and tools is strengthened, and innovative mechanisms for introducing ultrasonic enhancement are created to lower manufacturing costs and shorten reinforcement periods, promoting the application of ultrasonic enhancement technology in aerospace, deep-sea, and medical fields. At the same time, techniques such as big data, simulation, and machine learning should be utilized to optimize process parameters, establish theoretical models, and achieve precise control over remanufactured parts, driving the development of surface engineering and remanufacturing technologies.

## Funding

This work was supported financially by the National Natural Science Foundation of China (Grant No.: 52275228; 52475224).

## Data Availability

Not applicable.

## Conflicts of Interest

The authors declare no conflict of interest.

## References

- [1] X. G. Yang, M. L. Wang, D. Q. Shi, Z. L. Li, and Y. S. Fan, “A multi-scale framework for life reduction assessment of turbine blade caused by microstructural degradation,” *Chin. J. Aeronaut.*, vol. 37, no. 1, pp. 186–200, 2024. <https://doi.org/10.1016/j.cja.2023.07.021>
- [2] S. L. Zhu, J. C. Cong, W. Yuan, Q. J. Guo, X. J. Yao, B. T. Chi, and A. G. Yan, “Simulation of heavy-duty crankshaft sub-dynamics and experimental study of wear mechanisms,” *Mater. Today Commun.*, vol. 36, p. 106826, 2023. <https://doi.org/10.1016/j.mtcomm.2023.106826>
- [3] S. L. Zhu, W. Yuan, J. C. Cong, Q. J. Guo, B. T. Chi, and J. Yu, “Analysis of regional wear failure of crankshaft pair of heavy duty engine,” *Eng. Fail. Anal.*, vol. 154, p. 107635, 2023. <https://doi.org/10.1016/j.engfailanal.2023.107635>
- [4] Y. Lv, L. Q. Lei, L. N. Sun, and B. Cui, “Improvement of the wear resistance of 20CrMnTi steel gear by discrete laser surface melting,” *Opt. Laser Technol.*, vol. 165, p. 109598, 2023. <https://doi.org/10.1016/j.optlastec.2023.109598>
- [5] X. B. Li, J. Liu, J. Xu, Y. Chen, Z. Hu, and G. Pan, “A vibration model of a planetary bearing system considering the time-varying wear,” *Nonlinear Dyn.*, vol. 111, no. 21, p. 19840, 2023. <https://doi.org/10.1007/s11071-023-08845-5>
- [6] A. I. Balitskii, Y. H. Kvasnytska, L. M. Ivaskevych, K. H. Kvasnytska, O. A. Balitskii, I. A. Shalevska, O. Y. Shynskii, J. M. Jaworski, and J. M. Dowejko, “Hydrogen and corrosion resistance of nickel superalloys for gas turbines, engines cooled blades,” *Energies*, vol. 16, no. 3, p. 1154, 2023. <https://doi.org/10.3390/en16031154>
- [7] A. H. I. Mourad, A. Almomani, I. A. Sheikh, and A. H. Elsheikh, “Failure analysis of gas and wind turbine blades: A review,” *Eng. Fail. Anal.*, vol. 146, p. 107107, 2023. <https://doi.org/10.1016/j.engfailanal.2023.107107>

- [8] I. A. A. Bakar, N. I. Omar, Y. Yusuf, and T. A. Rahim, “Reflection and future perspectives in cold spray technology: A bibliometric analysis,” *J. Therm. Spray Tech.*, vol. 32, no. 6, pp. 1576–1595, 2023. <https://doi.org/10.1007/s11666-023-01612-3>
- [9] D. H. L. Seng, Z. Zhang, Z. Q. Zhang, T. L. Meng, S. L. Teo, B. H. Tan, Q. Z. Loi, J. S. Pan, and T. Ba, “Impact of spray angle and particle velocity in cold sprayed IN718 coatings,” *Surf. Coat. Tech.*, vol. 466, p. 129623, 2023. <https://doi.org/10.1016/j.surfcoat.2023.129623>
- [10] L. Z. Cheng, H. Chuang, and K. D. Jun, “Effect of laser remelting on microstructure, salt spray corrosion and electrochemical performance of plasma sprayed CoCrFeNiMo HEA coating,” *J. Mater. Sci.*, vol. 58, no. 25, pp. 10 484–10 500, 2023. <https://doi.org/10.1007/s10853-023-08638-6>
- [11] J. Yao, F. Liu, X. P. Wang, H. B. Liu, T. He, W. X. Dai, L. M. Tan, L. Huang, and Y. Liu, “Enhancing comprehensive properties of HVOF thermally sprayed WC-10Co coatings using two grain inhibitors,” *Surf. Coat. Tech.*, vol. 477, p. 130323, 2024. <https://doi.org/10.1016/j.surfcoat.2023.130323>
- [12] R. Gopi, I. Saravanan, A. Devaraju, and P. Sivasamy, “A review on recent progress in PVD-TiN coatings,” *Diffus. Found. Mater. Appl.*, vol. 34, pp. 41–53, 2023. <https://doi.org/10.4028/p-31Wzme>
- [13] B. Peng, Y. X. Xu, Z. H. Fan, and Q. M. Wang, “Oxidation behavior at 1100°C of NiCrAlY coatings deposited by various PVD techniques,” *Surf. Coat. Tech.*, vol. 477, p. 130307, 2024. <https://doi.org/10.1016/j.surfcoat.2023.130307>
- [14] L. Zhou, G. Z. Ma, H. C. Zhao, H. L. Mou, J. F. Xu, W. Z. Wang, Z. G. Xing, Y. Li, W. L. Guo, and H. D. Wang, “Research status and prospect of extreme high-speed laser cladding technology,” *Opt. Laser Technol.*, vol. 168, p. 109800, 2024. <https://doi.org/10.1016/j.optlastec.2023.109800>
- [15] W. Zhuang, Q. Liu, R. Djugum, P. K. Sharp, and A. Paradowska, “Deep surface rolling for fatigue life enhancement of laser clad aircraft aluminium alloy,” *Appl. Surf. Sci.*, vol. 320, pp. 558–562, 2014. <https://doi.org/10.1016/j.apsusc.2014.09.139>
- [16] Z. X. Chen, H. M. Zhou, Z. M. Zhu, C. X. Xu, and Y. M. Zhou, “Laser cladding remanufacturing of aircraft landing gear based on 30CrMnSiNi2A steel,” *Optik*, vol. 283, p. 170902, 2023. <https://doi.org/10.1016/j.ijleo.2023.170902>
- [17] S. C. Zhu, W. L. Chen, X. H. Zhan, L. P. Ding, and E. H. Wang, “Optimization of dilution rate of laser cladding repair based on deep learning,” *Int. J. Adv. Manuf. Technol.*, vol. 110, pp. 1471–1484, 2020. <https://doi.org/10.1007/s00170-020-05969-5>
- [18] W. Y. Yuan, R. F. Li, Z. H. Chen, J. Y. Gu, and Y. T. Tian, “A comparative study on microstructure and properties of traditional laser cladding and high-speed laser cladding of Ni45 alloy coatings,” *Surf. Coat. Tech.*, vol. 405, p. 126582, 2021. <https://doi.org/10.1016/j.surfcoat.2020.126582>
- [19] W. Gao, S. C. Wang, K. K. Hu, X. Z. Jiang, H. Y. Yu, and D. B. Sun, “Effect of laser cladding speed on microstructure and properties of titanium alloy coating on low carbon steel,” *Surf. Coat. Tech.*, vol. 451, p. 129029, 2022. <https://doi.org/10.1016/j.surfcoat.2022.129029>
- [20] X. L. Wang, A. R. Huang, C. J. Shang, and Z. J. Xie, “Characterization of the cladding layer by laser cladding of 9Cr18Mo powder on 3Cr14 martensitic stainless steel and the impact of martensite obtained through post heat treatment on hardness,” *Mater. Today Commun.*, vol. 32, p. 104057, 2022. <https://doi.org/10.1016/j.mtcomm.2022.104057>
- [21] Y. T. Li, H. G. Fu, K. M. Wang, X. J. Yang, B. Zong, and J. Lin, “Effect of Mo addition on microstructure and wear resistance of laser clad AlCoCrFeNi-TiC composite coatings,” *Appl. Surf. Sci.*, vol. 623, p. 157071, 2023. <https://doi.org/10.1016/j.apsusc.2023.157071>
- [22] H. L. Song, F. C. Jiang, C. H. Guo, Q. Sun, H. X. Li, Z. L. Yang, L. Y. Li, M. X. Diao, and Z. C. Zhang, “Effect of ultrasonic vibration on the microstructure and microhardness of laser cladding Fe-based crystalline/amorphous composite coatings,” *Mater. Lett.*, vol. 335, p. 133780, 2023. <https://doi.org/10.1016/j.matlet.2022.133780>
- [23] H. S. Chen, Z. Y. Zhang, J. M. Zhang, H. B. Ji, Z. Meng, H. Zhang, and X. K. Meng, “Effect of ultrasonic impact strengthening on surface properties of 316L stainless steel prepared by laser selective melting,” *Coatings*, vol. 12, no. 9, p. 1243, 2022. <https://doi.org/10.3390/coatings12091243>
- [24] Z. Q. Cui, Z. Qin, P. Dong, Y. J. Mi, D. Q. Gong, and W. G. Li, “Microstructure and corrosion properties of FeCoNiCrMn high entropy alloy coatings prepared by high speed laser cladding and ultrasonic surface mechanical rolling treatment,” *Mater. Lett.*, vol. 259, p. 126769, 2020. <https://doi.org/10.1016/j.matlet.2019.126769>
- [25] A. U. H. Mohsan, M. N. Zhang, D. F. Wang, S. Zhao, Y. S. Wang, C. Y. Chen, and J. H. Zhang, “State-of-the-art review on the Ultrasonic Vibration Assisted Laser Cladding (UVALC),” *J. Manuf. Processes*, vol. 107, pp. 422–446, 2023. <https://doi.org/10.1016/j.jmapro.2023.10.066>
- [26] S. Kumar, C. S. Wu, G. K. Padhy, and W. Ding, “Application of ultrasonic vibrations in welding and metal processing: A status review,” *J. Manuf. Processes*, vol. 26, pp. 295–322, 2017. <https://doi.org/10.1016/j.jmapro.2017.02.027>

- [27] M. Y. Li, B. Han, Y. Wang, L. X. Song, and L. Y. Guo, “Investigation on laser cladding high-hardness nano-ceramic coating assisted by ultrasonic vibration processing,” *Optik*, vol. 127, no. 11, pp. 4596–4600, 2016. <https://doi.org/10.1016/j.ijleo.2016.01.194>
- [28] Y. Z. Zhang, G. F. Hu, L. L. Zuo, M. L. Bang, N. Wang, D. G. Li, Z. H. Li, R. S. Li, W. W. He, B. C. Xue, and Y. Q. Zhang, “Ultrasonic vibration micro-jet ejection for metal additive manufacture,” *J. Mater. Res. Tech.*, vol. 28, pp. 2149–2162, 2024. <https://doi.org/10.1016/j.jmrt.2023.12.156>
- [29] F. Wang, D. G. Eskin, J. W. Mi, C. N. Wang, B. Koe, A. King, C. Reinhard, and T. Connolley, “A synchrotron X-radiography study of the fragmentation and refinement of primary intermetallic particles in an Al-35 Cu alloy induced by ultrasonic melt processing,” *Acta Mater.*, vol. 141, pp. 142–153, 2017. <https://doi.org/10.1016/j.actamat.2017.09.010>
- [30] B. Wang, D. Y. Tan, T. L. Lee, J. C. Khong, F. Wang, D. G. Eskin, T. Connolley, K. Fezzaa, and J. W. Mi, “Ultrafast synchrotron X-ray imaging studies of microstructure fragmentation in solidification under ultrasound,” *Acta Mater.*, vol. 144, pp. 505–515, 2018. <https://doi.org/10.1016/j.actamat.2017.10.067>
- [31] D. D. Zhuang, B. Du, S. H. Zhuang, W. W. Tao, Q. Wang, and H. B. Shen, “Effect and action mechanism of ultrasonic assistance on microstructure and mechanical performance of laser cladding 316L stainless steel coating,” *Surf. Coat. Tech.*, vol. 433, p. 128122, 2022. <https://doi.org/10.1016/j.surfcoat.2022.128122>
- [32] M. Jin, D. Y. He, W. Shao, Z. Tan, Q. Cao, X. Y. Guo, Z. Zhou, L. Cui, and L. Zhou, “The microstructure and high-temperature oxidation resistance of Si-rich Mo-Si-B coatings prepared by ultrasonic vibration assisted laser cladding,” *J. Alloys Compd.*, vol. 953, p. 170175, 2023. <https://doi.org/10.1016/j.jallcom.2023.170175>
- [33] J. Lv, J. Z. Zhou, X. K. Meng, P. F. Li, and S. Huang, “Microstructure and wear properties of IN718/WC composite coating fabricated by ultrasonic vibration-assisted laser cladding,” *Coatings*, vol. 12, no. 3, p. 412, 2022. <https://doi.org/10.3390/coatings12030412>
- [34] K. Qi, Y. Yang, G. F. Hu, X. Lu, and J. D. Li, “Thermal expansion control of composite coatings on 42CrMo by laser cladding,” *Surf. Coat. Tech.*, vol. 397, p. 125983, 2020. <https://doi.org/10.1016/j.surfcoat.2020.125983>
- [35] L. D. Zhu, Z. C. Yang, B. Xin, S. H. Wang, G. R. Meng, J. S. Ning, and P. S. Xue, “Microstructure and mechanical properties of parts formed by ultrasonic vibration-assisted laser cladding of Inconel 718,” *Surf. Coat. Tech.*, vol. 410, p. 126964, 2021. <https://doi.org/10.1016/j.surfcoat.2021.126964>
- [36] L. Yu and X. F. Liu, “The relationship between viscosity and refinement efficiency of pure aluminum by Al-Ti-B refiner,” *J. Alloys Compd.*, vol. 425, no. 1-2, pp. 245–250, 2006. <https://doi.org/10.1016/j.jallcom.2006.08.257>
- [37] J. Z. Wang, J. Z. Zhou, T. Zhang, X. K. Meng, P. F. Li, S. Huang, and H. Zhu, “Ultrasonic-induced grain refinement in laser cladding nickel-based superalloy reinforced by WC particles,” *Coatings*, vol. 13, no. 1, p. 151, 2023. <https://doi.org/10.3390/coatings13010151>
- [38] M. Zhang, G. L. Zhao, X. H. Wang, S. S. Liu, and W. L. Ying, “Microstructure evolution and properties of in-situ ceramic particles reinforced Fe-based composite coating produced by ultrasonic vibration assisted laser cladding processing,” *Surf. Coat. Tech.*, vol. 403, p. 126445, 2020. <https://doi.org/10.1016/j.surfcoat.2020.126445>
- [39] G. F. Hu, Y. Yang, X. Lu, and J. D. Li, “A study on the influence mechanism and optimization of physical field parameters of electromagnetic-ultrasonic compound field-assisted laser cladding technology,” *Weld. World*, vol. 65, no. 9, pp. 1687–1700, 2021. <https://doi.org/10.1007/s40194-021-01144-w>
- [40] A. H. Jabbari and M. Sedighi, “Investigation of electromagnetic and mechanical stirring sequence effects on production of magnesium matrix nanocomposite,” *Inter. Metalcast.*, vol. 14, no. 2, pp. 489–504, 2020. <https://doi.org/10.1007/s40962-019-00374-5>
- [41] G. F. Hu, Y. Yang, R. Sun, K. Qi, X. Lu, and J. D. Li, “Microstructure and properties of laser cladding NiCrBSi coating assisted by electromagnetic-ultrasonic compound field,” *Surf. Coat. Tech.*, vol. 404, p. 126469, 2020. <https://doi.org/10.1016/j.surfcoat.2020.126469>
- [42] T. Zhang, P. F. Li, J. Z. Zhou, C. Y. Wang, X. K. Meng, and S. Huang, “Microstructure evolution of laser cladding Inconel 718 assisted hybrid ultrasonic-electromagnetic field,” *Mater. Lett.*, vol. 289, p. 129401, 2021. <https://doi.org/10.1016/j.matlet.2021.129401>
- [43] H. M. Zhou, Z. X. Chen, M. F. Li, Y. X. Zhu, C. X. Xu, and J. H. Zhou, “Effect of magnetic-electric-ultrasonic fields on microstructure and properties of Ni60A laser cladding coating,” *Mater. Lett. X*, vol. 14, p. 100132, 2022. <https://doi.org/10.1016/j.mlblux.2022.100132>
- [44] K. K. Zheng, Y. X. Lin, J. G. Cai, and C. Q. Lei, “Corrosion resistance and tribological properties of laser cladding layer of H13 die steel strengthened by ultrasonic rolling,” *Chin. J. Mech. Eng.*, vol. 35, no. 1, p. 137, 2022. <https://doi.org/10.1186/s10033-022-00810-4>
- [45] S. L. Lan, M. Qi, Y. F. Zhu, M. X. Liu, and W. B. Bie, “Ultrasonic rolling strengthening effect on the bending fatigue behavior of 12Cr2Ni4A steel gears,” *Eng. Fract. Mech.*, vol. 279, p. 109024, 2023. <https://doi.org/10.1016/j.engfracmech.2022.109024>
- [46] J. H. Cong, J. Y. Gao, S. Zhou, N. J. Wang, J. H. Wang, and L. Hui, “Effect of ultrasonic rolling on crack

- propagation behavior of Ti6Al4V titanium alloy laser welded joints,” *Eng. Fract. Mech.*, vol. 292, p. 109618, 2023. <https://doi.org/10.1016/j.engfracmech.2023.109618>
- [47] Q. Z. Xu, D. W. Jiang, J. Zhou, Z. H. Qiu, and X. Yang, “Enhanced corrosion resistance of laser additive manufactured 316L stainless steel by ultrasonic surface rolling process,” *Surf. Coat. Tech.*, vol. 454, p. 129187, 2023. <https://doi.org/10.1016/j.surfcoat.2022.129187>
- [48] J. W. Xie, S. Q. Zhang, Y. A. Sun, Y. X. Hao, B. F. An, Q. L. Li, and C. A. Wang, “Microstructure and mechanical properties of high entropy CrMnFeCoNi alloy processed by electropulsing-assisted ultrasonic surface rolling,” *Mater. Sci. Eng. A*, vol. 795, p. 140004, 2020. <https://doi.org/10.1016/j.msea.2020.140004>
- [49] H. B. Wang, G. L. Song, and G. Y. Tang, “Enhanced surface properties of austenitic stainless steel by electropulsing-assisted ultrasonic surface rolling process,” *Surf. Coat. Tech.*, vol. 282, pp. 149–154, 2015. <https://doi.org/10.1016/j.surfcoat.2015.10.026>
- [50] Z. Y. Sun, Y. D. Ye, J. B. Xu, T. M. Hu, S. Ren, and B. Li, “Effect of electropulsing on surface mechanical behavior and microstructural evolution of Inconel 718 during ultrasonic surface rolling process,” *J. Materi. Eng. Perform.*, vol. 28, pp. 6789–6799, 2019. <https://doi.org/10.1007/s11665-019-04443-y>
- [51] Y. A. Sun, H. B. Wang, W. Liu, G. L. Song, and Q. L. Li, “Improvement of surface resistance to cavitation corrosion of nickel aluminum bronze by electropulsing-assisted ultrasonic surface rolling process,” *Surf. Coat. Tech.*, vol. 368, pp. 215–223, 2019. <https://doi.org/10.1016/j.surfcoat.2019.03.045>
- [52] G. Li, S. G. Qu, M. X. Xie, and X. Q. Li, “Effect of ultrasonic surface rolling at low temperatures on surface layer microstructure and properties of HIP Ti-6Al-4V alloy,” *Surf. Coat. Tech.*, vol. 316, pp. 75–84, 2017. <https://doi.org/10.1016/j.surfcoat.2017.01.099>
- [53] Z. H. Liu, L. S. Zheng, P. Tang, and S. W. Qin, “Investigation on surface integrity and process parameter optimisation of carburised 18CrNiMo7-6 steel by induction-heating-assisted ultrasonic surface rolling process,” *Int. J. Adv. Manuf. Technol.*, vol. 129, no. 3, pp. 1071–1086, 2023. <https://doi.org/10.1007/s00170-023-12301-4>
- [54] X. H. Shen, C. S. Zhang, H. Peng, C. Liu, and Y. Zhang, “Achieving high surface integrity of Fe-based laser cladding coating by optimized temperature field-assisted ultrasonic burnishing,” *J. Manuf. Processes*, vol. 83, pp. 270–280, 2022. <https://doi.org/10.1016/j.jmapro.2022.08.047>
- [55] J. Zhang, Y. C. Zhao, Y. He, C. Meng, X. Y. Zhang, and S. L. Zhang, “Effect of high-temperature-assisted ultrasonic deep rolling on microstructure and tribological properties of Ni-WC coatings,” *Coatings*, vol. 13, no. 3, p. 499, 2023. <https://doi.org/10.3390/coatings13030499>
- [56] X. S. Luan, W. X. Zhao, Z. Q. Liang, S. H. Xiao, G. X. Liang, Y. F. Chen, S. K. Zou, and X. B. Wang, “Experimental study on surface integrity of ultra-high-strength steel by ultrasonic hot rolling surface strengthening,” *Surf. Coat. Tech.*, vol. 392, p. 125745, 2020. <https://doi.org/10.1016/j.surfcoat.2020.125745>
- [57] D. A. Lesyk, S. Martinez, B. N. Mordyuk, V. V. Dzhemelinskyi, A. Lamikiz, and G. I. Prokopenko, “Post-processing of the Inconel 718 alloy parts fabricated by selective laser melting: Effects of mechanical surface treatments on surface topography, porosity, hardness and residual stress,” *Surf. Coat. Tech.*, vol. 381, p. 125136, 2020. <https://doi.org/10.1016/j.surfcoat.2019.125136>
- [58] Y. C. Wang and J. Shi, “Microstructure and properties of Inconel 718 fabricated by directed energy deposition with in-situ ultrasonic impact peening,” *Metall. Mater. Trans. B*, vol. 50, pp. 2815–2817, 2019. <https://doi.org/10.1007/s11663-019-01672-3>
- [59] C. S. Wang, R. F. Li, X. L. Bi, W. Y. Yuan, J. Y. Gu, J. Chen, M. J. Yan, and Z. Y. Zhang, “Microstructure and wear resistance property of laser cladded CrCoNi coatings assisted by ultrasonic impact treatment,” *J. Mater. Res. Technol.*, vol. 22, pp. 853–864, 2023. <https://doi.org/10.1016/j.jmrt.2022.11.170>
- [60] S. Y. Zhang, B. Han, M. Y. Li, C. Y. Hu, Q. Zhang, X. F. Liu, and Y. Wang, “Investigation on microstructure and properties of laser cladded AlCoCrCuFeNi high entropy alloy coating by ultrasonic impact treatment,” *Intermetallics*, vol. 128, p. 107017, 2021. <https://doi.org/10.1016/j.intermet.2020.107017>
- [61] Z. H. Song, S. X. Liu, X. W. Qiu, L. T. Zhang, C. Wu, X. Ren, X. L. Wang, and C. Meng, “Effect of ultrasonic impact treatment on the properties of CoCrFeNiCu high-entropy alloy coatings on steel by induction cladding,” *Surf. Coat. Tech.*, vol. 459, p. 129390, 2023. <https://doi.org/10.1016/j.surfcoat.2023.129390>
- [62] D. Y. Lin, L. Y. Xu, H. Y. Jing, Y. D. Han, L. Zhao, and F. Minami, “Effects of annealing on the structure and mechanical properties of FeCoCrNi high-entropy alloy fabricated via selective laser melting,” *Addit. Manuf.*, vol. 32, p. 101058, 2020. <https://doi.org/10.1016/j.addma.2020.101058>
- [63] J. H. Martin, B. D. Yahata, J. M. Hundley, J. A. Mayer, T. A. Schaedler, and T. M. Pollock, “3D printing of high-strength aluminium alloys,” *Nature*, vol. 549, no. 7672, pp. 365–369, 2017. <https://doi.org/10.1038/nature23894>
- [64] M. X. Zhang, C. M. Liu, X. Z. Shi, X. P. Chen, C. Chen, J. H. Zuo, J. P. Lu, and S. Y. Ma, “Residual stress, defects and grain morphology of Ti-6Al-4V alloy produced by ultrasonic impact treatment assisted selective laser melting,” *Appl. Sci.*, vol. 6, no. 11, p. 304, 2016. <https://doi.org/10.3390/app6110304>
- [65] S. W. Hua, M. Pang, F. Q. Ji, J. Chen, and G. Liu, “Microstructure and tribological properties of Ti2AlC-B

- particle-enhanced self-lubricating coatings on Ti6Al4V by ultrasonic impact treatment and laser cladding,” *Mater. Today Commun.*, vol. 34, p. 105165, 2023. <https://doi.org/10.1016/j.mtcomm.2022.105165>
- [66] M. Y. Li, Q. Zhang, B. Han, L. X. Song, J. L. Li, and J. Yang, “Investigation on microstructure and properties of Al<sub>x</sub>CoCrFeMnNi high entropy alloys by ultrasonic impact treatment,” *J. Alloys Compd.*, vol. 816, p. 152626, 2020. <https://doi.org/10.1016/j.jallcom.2019.152626>
- [67] E. Emelianova, V. Romanova, O. Zinovieva, and R. Balokhonov, “The effects of surface-layer grain size and texture on deformation-induced surface roughening in polycrystalline titanium hardened by ultrasonic impact treatment,” *Mater. Sci. Eng. A*, vol. 793, p. 139896, 2020. <https://doi.org/10.1016/j.msea.2020.139896>
- [68] T. T. He, Z. M. Ding, C. B. Shen, and Z. Li, “Mechanisms and characteristics of ultrasonic impact treatment on steel surface,” *Adv. Mater. Res.*, vol. 834-836, pp. 649–653, 2013. <https://doi.org/10.4028/www.scientific.net/A MR.834-836.649>
- [69] Y. Z. Zhang, C. P. Huang, F. G. Liu, F. C. Liu, M. H. Song, and L. M. Ke, “Nanocrystallization of a Ti40 cladding layer by ultrasonic impact to improve burn resistance,” *J. Mater. Res. Technol.*, vol. 11, pp. 1331–1342, 2021. <https://doi.org/10.1016/j.jmrt.2021.01.083>
- [70] R. Rui, J. F. Fan, B. S. Wang, Q. Zhang, W. G. Li, and H. B. Dong, “Hall-Petch relationship and deformation mechanism of pure Mg at room temperature,” *J. Alloys Compd.*, vol. 920, p. 165924, 2022. <https://doi.org/10.1016/j.jallcom.2022.165924>
- [71] N. Hansen, “Hall-Petch relation and boundary strengthening,” *Scripta Mater.*, vol. 51, no. 8, pp. 801–806, 2004. <https://doi.org/10.1016/j.scriptamat.2004.06.002>
- [72] J. Zhang, C. J. Zhao, Q. F. Bai, Q. H. Li, C. Chen, and J. G. Liang, “Effect of ultrasonic high-frequency percussion on the microstructure and corrosion resistance of Fe-based alloy coatings by high-speed laser cladding,” *Mater. Lett.*, vol. 335, p. 133769, 2023. <https://doi.org/10.1016/j.matlet.2022.133769>
- [73] D. A. Lesyk, B. N. Mordyuk, S. Martinez, M. O. Iefimov, V. V. Dzhemelinskyi, and A. Lamikiz, “Influence of combined laser heat treatment and ultrasonic impact treatment on microstructure and corrosion behavior of AlSi 1045 steel,” *Surf. Coat. Tech.*, vol. 401, p. 126275, 2020. <https://doi.org/10.1016/j.surfcoat.2020.126275>
- [74] M. Y. Li, Q. Zhang, B. Han, L. X. Song, J. L. Li, and S. Y. Zhang, “Effects of ultrasonic impact treatment on structures and properties of laser cladding Al0.5CoCrFeMnNi high entropy alloy coatings,” *Mater. Chem. Phys.*, vol. 258, p. 123850, 2021. <https://doi.org/10.1016/j.matchemphys.2020.123850>
- [75] A. I. Dekhtyar, B. N. Mordyuk, D. G. Savvakin, V. I. Bondarchuk, I. V. Moiseeva, and N. I. Khripta, “Enhanced fatigue behavior of powder metallurgy Ti–6Al–4V alloy by applying ultrasonic impact treatment,” *Mater. Sci. Eng. A*, vol. 641, pp. 348–359, 2015. <https://doi.org/10.1016/j.msea.2015.06.072>
- [76] J. S. Jesus, L. P. Borrego, J. A. M. Ferreira, J. D. Costa, and C. Capela, “Fatigue crack growth behaviour in Ti6Al4V alloy specimens produced by selective laser melting,” *Int. J. Fract.*, vol. 223, no. 1, pp. 123–133, 2020. <https://doi.org/10.1007/s10704-019-00417-2>
- [77] A. V. Eremin, M. V. Burkov, S. V. Panin, and A. V. Byakov, “Fatigue crack growth of SLM Ti-4Al-6V processed by ultrasonic impact treatment,” *AIP Conf. Proc.*, vol. 2167, no. 1, p. 020082, 2019. <https://doi.org/10.1063/1.5131949>
- [78] P. Walker, S. Malz, E. Trudel, S. Nosir, M. S. A. ElSayed, and L. Kok, “Effects of ultrasonic impact treatment on the stress-controlled fatigue performance of additively manufactured DMLS Ti-6Al-4V alloy,” *Appl. Sci.*, vol. 9, no. 22, p. 4787, 2019. <https://doi.org/10.3390/app9224787>